Galleria mellonella as an infection model for the virulent *Mycobacterium tuberculosis* H37Rv

Short title: Insect infection model for *M. tuberculosis* H37Rv

Masanori Asai[1*], Yanwen Li[1], John Spiropoulos[2], William Cooley[2], David J. Everest[2], Sharon L. Kendall[3], Carlos Martín[4], Brian D. Robertson[5], Paul R. Langford[1+], Sandra M. Newton[1+]

[1] Section of Paediatric Infectious Diseases, Department of Infectious Disease, Imperial College London, London, UK

[2] Department of Pathology, Animal and Plant Health Agency, Addlestone, UK

[3]Centre for Emerging, Endemic and Exotic Diseases, Pathobiology and Population Sciences, Royal Veterinary College, Hartfield, UK

[4]Department of Microbiology, Facultad de Medicina Universidad de Zaragoza, CIBERES, (ISCIII), Spain

[5] MRC Centre for Molecular Bacteriology and Infection, Department of Infectious Disease, Imperial College London, UK

[+] Joint co-author

*Correspondence:

Dr Masanori Asai

m.asai16@imperial.ac.uk

Abstract

Tuberculosis (TB), caused by *Mycobacterium tuberculosis* (*MTB*), is a leading cause of infectious disease mortality. Animal infection models have contributed substantially to our understanding of TB, yet their biological and non-biological limitations are a research bottleneck. There is a need for more ethically acceptable, economical, and reproducible TB infection models capable of mimicking key aspects of disease. Here we demonstrate and present a basic description of how *Galleria mellonella* (the greater wax moth, *Gm*) larvae can be used as a low cost, rapid and ethically more acceptable model for TB research. This is the first study to infect *Gm* with the fully virulent *MTB* H37Rv, the most widely used strain in research. Infection of *Gm* with *MTB* resulted in a symptomatic lethal infection, the virulence of which differed from both attenuated *Mycobacterium bovis* BCG and auxotrophic *MTB* strains. The *Gm-MTB* model can also be used for anti-TB drug screening, although CFU enumeration from *Gm* is necessary for confirmation of mycobacterial load reducing activity of the tested compound. Furthermore, comparative virulence of *MTB* isogenic mutants can be determined in *Gm*. However, comparison of mutant phenotypes in Gm against conventional models must consider the limitations of innate immunity. Our findings indicate that *Gm* will be a practical, valuable and advantageous additional model to be used alongside existing models to advance tuberculosis research.

Key words: Tuberculosis, *Mycobacterium tuberculosis*, *Galleria mellonella*, infection model, innate immunity, mycobacteria

Introduction

Tuberculosis (TB) is caused by *Mycobacterium tuberculosis* (*MTB*) (1). Conventional animal models of TB have both biological (capacity to mimic aspects of disease, e.g., induction of granulomas) and non-biological (acquisition and maintenance cost, animal housing and ethical restrictions) limitations that are bottlenecks in research (2). While alternative and ethically more acceptable infection models such as zebrafish (3) and fruit flies (4) are available, these models require the use of surrogate mycobacterial species such as *Mycobacterium marinum* and may be associated with different responses to that induced by *MTB*. Thus, there is a need for alternative *MTB* models that replicate key aspects of disease including granuloma formation, the hallmark of human TB (5).

The larvae of *Galleria mellonella* (*Gm*) are a potential infection model (6). As a model to study infectious disease *Gm* has already been described with over 65 bacterial and fungal pathogens, with over 1500 articles registered on NCBI PubMed in the last decade alone (search terms: *Galleria mellonella* AND infection). Uptake in *Gm* as an infection model stems from a number of advantageous properties. *Gm* possess a complex innate immune system comprised of phagocytic cells (haemocytes), that function similarly to mammalian neutrophils and macrophages. Unlike zebrafish or fruit flies, *Gm* can be incubated at 37 °C, and do not require specialised maintenance facilities or equipment. Infections are typically conducted via injection which allows for accurate dosing of pathogens. This is important considering that virulence in *Gm* can often vary widely with small differences (e.g., 0.5 log CFU) in infectious dose (7–10). *Gm* are cost-effective, their short lifespan facilitates rapid acquisition of reproducible data, and ethical approval is not required. However, as a model organism in its infancy, the experimental capability of *Gm* is limited by the lack of widely accessible immunological and molecular methods/toolbox for comprehensive characterisation of the host response to infection.

Previously, we infected *Gm* with members of the *MTB* complex (MTBC), i.e., *Mycobacterium bovis* BCG Montréal (BCG *lux*) (11), and a biosafety level (BSL)-2 compliant double auxotroph of *MTB* (Δ*leuD* Δ*panCD,* SAMTB *lux*) (12). These mycobacteria induced larval mortality, were internalised by haemocytes, survived *in vivo*, induced the formation of granuloma-like structures (GLS), and the models facilitated screening for antimycobacterial compounds (12, 13). While SAMTB *lux*, unlike BCG *lux,* preserved the virulence locus RD1 but both mycobacteria were equally virulent in *Gm* (14). This raised concerns that *Gm* could not differentiate the virulence between the members of the MTBC and/or their isogenic mutants. Additionally, feedback from the TB community indicated concerns about the relevance of relatively high doses and short time frame used in the published studies (11–13, 15, 16).

To address these concerns, we report here for the first time, infection of *Gm* with the widely used virulent *MTB* strain H37Rv (17), the parental strain of SAMTB *lux* (12, 18). H37Rv originates from the clinical isolate H37, isolated from a TB patient at the Trudeau Institute in 1905 (19). H37 has evolved into two strains, the avirulent H37Ra and the virulent H37Rv (20), with the latter adopted as a reference strain due to its phenotypic similarities with the tubercule bacilli described by Robert Koch (17). Here, we describe a revised infection model utilising a lower infectious dose and extended study length which differentiates mycobacterial virulence in the order of virulence is H37Rv >SAMTB *lux*

>BCG *lux*; includes the presence of GLS in response to H37Rv, can be used as a screen for anti-TB drugs, and as a virulence screen for isogenic *MTB* mutants.

Results

Infection with H37Rv leads to bacterial proliferation and is more lethal for G. mellonella compared to BCG lux and *SAMTB lux*

Gm larvae were challenged with varying CFU doses of H37Rv to determine virulence as described (11–13, 16). Larval mortality positively correlated with increasing CFU dose (**Figure 1a**), where the LD_{50} (infectious dose killing 50% population over 192 h) was 2 x 10^6 CFU. Infection with non-viable heat-treated (HT) H37Rv (2 x 10^6 CFU) failed to induce significant larval mortality, indicating virulence required viable bacteria (**Figure 1a**). No adverse effects were seen in *Gm* mock-infected with phosphate buffered saline (PBS) containing 0.05% of Tween-80 (PBS-T). Bacterial infection led to symptomatic disease: melanisation (darkening of cuticle), reduced motility, and death. The incubation time prior to symptomatic disease increased as CFU dose reduced. The survival of H37Rv (2 x 10^6 CFU) in *Gm* was evaluated by CFU enumeration from larval homogenates. H37Rv established a proliferative infection in *Gm* with ~1.1 log CFUs increase over 192 h (**Figure 1b**). Mycobacterial load increased substantially (~0.90 log CFUs) within the first 96 h post-infection (pi). Between 96 and 192 h pi, mycobacterial growth declined noticeably (~0.20 log CFUs). The virulence of H37Rv was compared against BCG *lux* and SAMTB *lux* under two experimental conditions: original and revised. The "original" parameter utilised a starting inocula of 10^7 CFU over 96 h (**Figure 1c,** 192 h time-course is available as **Supplementary Figure 1**). The "revised" parameter used 10^6 CFU over 192 h (**Figure 1d**). The "original" parameter reflected the LD_{50} doses previously defined for *Gm* infection which were 1 x 10^7 CFU and 2 x 10^7 CFU, respectively for BCG *lux* (11, 13, 15, 16) and SAMTB *lux* (12) over 96 h. For H37Rv, 1 x 10^7 CFU was utilised for the original parameter. For the revised model, *Gm* were infected with BCG *lux*/SAMTB *lux*/H37Rv at 2 x 10^6 CFU. At both doses, H37Rv was more virulent than BCG *lux* (10^6 CFU: $p < 0.0001$ and 10^7 CFU: trend but not significant), and SAMTB *lux* (10^6 CFU: $p < 0.001$ and 10^7 CFU: $p < 0.05$). Significant differences in survival between BCG *lux* and SAMTB *lux* were observed at 10^6 CFU ($p < 0.05$), but not with 10^7 CFU. These results indicate that differences in virulence between members of the MTBC were found in *Gm* in a dose-dependent manner.

H37Rv is internalised in haemocytes and induces the formation of GLS throughout the larval cavity

Internalisation of H37Rv by haemocytes was visualised by transmission electron microscopy (TEM) as early as 1 h pi (**Figure 2a**). By 24 h pi, haemocyte aggregates containing small clusters of bacilli were apparent (**Figure 2b**). By 96 h pi, haemocytes surrounding a large central mass of bacilli became more common (**Figure 2c**). With disease progression, individual haemocytes appeared to contain larger numbers of bacilli (**Figure 2d**). By 192 h pi, haemocytes appear necrotic, as adjudged by loss of cell integrity and leakage of intracellular materials (**Figure 2e**). Intracellular bacilli were observable at all time-points, supporting the proliferative nature of the infection as determined by CFU enumeration. Intracellular H37Rv lacked any distinguishable changes in their phenotype such as formation of intracytosolic lipid inclusions (ILIs).

GLS were found in increasing frequency and size during infection throughout the larval cavity as shown by Ziehl-Neelsen (ZN) staining of sagittal whole larval sections (**Figure 3 and 4**). These GLS comprise *Gm* cells organised around clusters or foci of H37Rv (**Figure 4b**). Both viable (pink ZN staining) and dead/decaying (dense purple ZN-masses lacking defined shape) bacilli were present. Corresponding sections stain intensely with Haematoxylin and Eosin (H&E) (**Figure 4a**), indicating host cellular necrosis. Following initial containment, mycobacteria were found in small aggregates within GLS at 48 h pi, (**Figure 4d**), in less complex arrangements compared to those at 24 h pi. H&E staining at 48 h indicated minimal levels of host necrosis (**Figure 4c**). At later timepoints, H37Rv appeared to replicate within GLS, as indicated by the abundance of pink ZN-stained bacilli (144 h pi, **Figure 4h**). The corresponding 144 h H&E-stained section shows *Gm* cells forming a clear border surrounding infected *Gm* cells, characterised by a circular eosinophilic area with faded spongy pockets of staining (**Figures 4g and 5a**). Furthermore, GLS contained melanised (brown/black) residues of probable digested mycobacterial material (**Figure 4h**). By 192 h pi (**Figure 4j**), GLS contained a variety of infection foci, including melanised, proliferative, and dead/dying bacilli. As with other structures, areas of host necrosis co-localised with mycobacteria (**Figure 4i**). Interestingly, at 192 h, GLS containing primarily grey non-ZN-reactive masses were apparent (**Figure 4l**), a similar structure was identified as early as 96 h pi (**Figure 4f**), and peripheral loss of ZN-reactivity was also observed (highlighted in **Figures 4j and 5b)**. Relative to ZN-reactive foci, host cell nuclei were more clearly visualised in H&E stains of ZN negative foci (**Figures 4k and 5b, 5c**), indicating reduced host cell necrosis. These non-ZN-reactive foci were restricted to GLS which were well organised. The formation of GLS, *in vivo* proliferation of bacilli and larval mortality correlated with the change in the number of circulating haemocytes found within the infected larva over the course of infection (**Figure 6**).

The *G. mellonella*-H37Rv infection model can be used to determine antimycobacterial drug efficacy

The *Gm*-H37Rv infection model was evaluated as a screen for drug efficacy with established antimycobacterials using adult TB treatment doses (21) scaled relative to the body mass of *Gm* (200 mg): isoniazid (INH, 5 mg/kg), rifampicin (RIF, 10 mg/kg), ethambutol (ETH, 15 mg/kg) and pyrazinamide (PZA, 25 mg/kg). Supplementary Table 1 lists the MICs. A single compound/dose was injected 72 h pi. INH or RIF treatment led to significant improvements ($p < 0.0001$) in larval survival relative to mock-treated (PBS-T) control (**Supplementary Figure 2**). ETH and PZA failed to improve larval survival. Treatment with ETH 10x (150 mg/kg) resulted in non-significant improvements in larval survival (61 %, ETH 1x [37%]) relative to the PBS-T control (**Figure 7a**). No improvement in survival was observed with PZA 10x (250 mg/kg) treatment. At 120 h post-treatment there were significant reductions in H37Rv load ($p < 0.0001$) with INH, RIF, and ETH (10x) relative to the PBS-T control (**Figure 7b**). Only a 12 % reduction in CFU load was found with PZA (10x) relative to the control. The activity of INH, RIF and ETH was compared to mycobacterial load at the point of treatment (PT) (**Figure 7b**), and the CFUs recovered from the mock treated control as reference for growth and treatment activity (bactericidal or static). Relative to PT, INH and RIF treatment led to significant reductions in mycobacterial load ($p < 0.0001$ and $p < 0.001$, respectively), indicating bactericidal activity. For ETH, while a significant level of growth ($p < 0.001$) was detected relative to PT, a significant reduction ($p < 0.0001$) in CFUs relative to the mock treated control, indicates bacteriostatic activity.

***G. mellonella* can be used to distinguish relative virulence of H37Rv mutants**

The use of *Gm* as a screen for comparative *MTB* virulence, was evaluated using two isogenic H37Rv mutants, Δ*phoP* and Δ*dosR*, chosen based on their altered phenotype in traditional TB infection models, i.e., mice (22–27), guinea pigs (28), rabbits (25) and non-human primates (NHPs) (29). Virulence of these mutants was assessed in *Gm* at an infectious dose of 2×10^7 CFU, over 192 hrs. Larval challenge with Δ*phoP* led to significant ($p < 0.0001$) attenuation in virulence relative to the WT, with larval survival of 93% and 48%, respectively (**Figure 8a**). In contrast to Δ*phoP*, larval challenge with Δ*dosR* led to significant ($p < 0.01$) potentiation of virulence relative to WT, with larval survival of 30% and 53%, respectively (**Figure 8b**). For both Δ*phoP* and Δ*dosR*, larval challenge with complemented strains resulted in restoration of virulence to near WT levels (statistically not significant: 58% and 62% survival, respectively). Attenuation of Δ*phoP* and hypervirulence of Δ*dosR* were in-line with results reported in a severe combined immunodeficient (SCID) mouse infection model (22, 27).

Discussion

We have previously published BSL-2 compliant BCG *lux* (11) and SAMTB *lux* (12) infection models. However, subsequent TB community feedback raised concerns that use of surrogate strains was not equivalent to virulent *MTB*, and the incubation period was too short. Therefore, we have characterised a *Gm-MTB* infection model using fully virulent H37Rv (17), and compared this to our original BCG *lux* (11) and SAMTB *lux* (12) infection models with original (10^7 CFU) and revised (10^6 CFU) infectious doses, and an extended incubation period (96 h to 192 h). *Gm*-H37Rv infection with these revised infection parameters, resulted in proliferative infection similar to SAMTB *lux* (12). The revised parameters better reflect the chronic nature of TB, as the period prior to symptomatic disease is longer (+ 96 h relative to 10^7 CFU dose). Whilst this incubation period is shorter and the infectious dose is higher than those used in traditional mammalian models, it is commensurate with the short life span of *Gm* and with the advantages of the low cost, low maintenance, and speed.

Comparison of H37Rv, BCG *lux* and SAMTB *lux* virulence in *Gm*, with both original and revised infection parameters, found that mycobacterial virulence could be differentiated, but with some limitations. With the original parameters, the ability to differentiate virulence between H37Rv and BCG *lux* or SAMTB *lux* was limited, as no significant change in virulence was found between H37Rv and BCG *lux*. However, with revised infection parameters the comparative virulence order was H37Rv > SAMTB *lux* > BCG *lux*. Previously we hypothesized that the high abundance of *Gm* leucine and pantothenate (30, 31) allowed SAMTB *lux* to bypass the double auxotrophy for optimal growth (12). However, comparison with the H37Rv data, suggests that the double auxotrophy influences growth and virulence, although the mechanism is unknown. The use of other mycobacteria such as *Mycobacterium smegmatis* and other non-tuberculous mycobacteria (NTM) for comparison were considered. However, such comparison would be uninterpretable at the dosage and incubation period of this study, as the rate of multiplicity in NTMs are substantially higher than in the MTBC (32). Moreover, *M. smegmatis* (5×10^3 CFU) has already been studied in *Gm,* resulting in 80% larval survival after 17 days of incubation (33). Moreover, wide variety of NTMs have been screened, with all models having the capacity to differentiate between virulent and avirulent strains (10).

The use of commercially available *Gm* prevents for a lengthy study, as majority of non-lethal dose and control larvae begins to pupate and metamorphose into adult moth between 96-192 h. Our current

institutional guidelines prohibit the study of *Gm* beyond the larval stage, as adult moth are an environmental pest and flight risk adds to biohazardous challenges. Furthermore, while the larval stage does not require ethics approval, the pupal stage does and requires a separate pest licence for up keep. Based on our previous *Gm*-BCG *lux* proteomics study, there is a need for innate immune induction to inhibit larval pupation, and that involves the activity of the insect metalloprotease inhibitor (IMPI) protein which is known to regulate metamorphism (15). It is likely that lower doses of MTBC, unlike NTMs, do not inhibit pupation during our study duration, in part because of differences in rates of multiplication. Therefore, for study beyond the 192 h, researchers could utilise early instar larvae with longer lead time to pupation. However, such work requires rearing of an in-house *Gm* colony and feeding of infected larvae to ensure growth to last instar, both requiring additional time, resources and facilities, thereby removing major advantages of this model.

In immune-competent animal models with adaptive immunity, infection is regulated over time (34–36). However, lacking adaptive immunity, *Gm* relies on its innate immune response, controlling the rate of mycobacterial replication through cellular responses including phagocytosis and the formation of GLS (also known as nodulation or encapsulation)(37). These cellular responses are supported by the humoral response producing antimicrobial effectors such as antimicrobial peptides (AMPs), reactive species, phenolic compounds, and antimicrobial enzymes (e.g., lysozyme) (15, 38, 39). Evidence that the *Gm* immune response kills mycobacteria is seen by histological staining of dead/necrotic H37Rv, although the response is insufficient to control infection and, without additional input from adaptive immunity, *Gm* eventually succumbs to proliferative bacilli which are disseminated from the GLS (12). This narrative is supported by changes in Total Haemocyte Count (THC) in the circulation during the infection. During the non-symptomatic incubation period, haemocytes are recruited from the haemocoel to form GLS (40, 41), lowering the THC, implying active maintenance of GLS to contain the bacilli. Over time, GLS are overwhelmed, and bacilli released (96-168 h pi) inducting symptomatic disease. Dissemination of active bacilli from GLS into the extracellular environment stimulates larval immune response to increase the abundance of circulating haemocytes. Ultimately, immunity succumbs to the uncontrolled replication of bacilli, and a cascade of uncontrolled humoral responses, leading to death. Current study of the TB disease is limited to the acute phase of infection; represented by our study length and the uncontrolled mycobacterial replication in GLS, dissemination active bacilli and phagocytosis by haemocytes to develop GLS. However, while GLS are formed, it is unknown as to whether they are representative of those found in animals and humans, especially LTBI.

Previously, in the *Gm*-BCG *lux* model, ILIs were found in intracellular bacilli (11), and in mycobacteria recovered from granuloma-associated foamy macrophages (42). Their formation is triggered by intracellular stress, and are crucial energy source for survival during non-replicative infection (43). Such response by BCG *lux* in *Gm* was previously reported with the detection of mycobacterial diacylglycerol O-acyltransferase in the haemolymph (15), presence of which is classically associated with ILI formation (43). There was no ILI formation in intracellular H37Rv or intracellular SAMTB *lux* (12), perhaps reflecting the proliferative nature of the infection. The lack of ILIs in H37Rv and SAMTB *lux* may be attributable to the RD1 locus which BCG *lux* lacks (14). RD1 encodes the ESX-1 secretory system and 6 kDa early secretory antigenic target (ESAT-6), 10 kDa culture filtrate protein (CFP-10), required to escape the intracellular environment (44). Lacking RD1, BCG *lux* may preferentially induce the formation of ILIs as a stress response against oxidative and hypoxic stress, minimising damage from the intracellular environment, and maximising its chance of survival (45). Based on our observations in the BCG *lux* study, some mycobacteria have the potential to enter a persistent like state, as evident by ILI formation. However, its significance within the *Gm* model remains unclear, i.e., eventual degradation by host or reactivation.

While our TEM data confirmed the internalisation of mycobacteria by haemocytes, the identity of the receptor required to initiate mycobacterial phagocytosis is unknown and will remain so until the necessary tools to investigate such questions are developed for *Gm*. Only two of six haemocyte sub-types, plasmatocytes and granulocytes, are believed to be phagocytic (37). However, owing to the lack of markers required to differentiate the sub-types via fluorescence microscopy or flow cytometry, there are no accurate and reproducible methods enabling differentiation. While the phagocytic activity of haemocytes has been published (46–50), studies have assumed that all adherent cells are phagocytic and that non-adherent cells are non-phagocytic, which skews the data. This is evident from haemocyte comparison against neutrophils and macrophages, which reported reduced phagocytic uptake in haemocyte relative to their mammalian counterparts, where assays have not considered that not all adherent cells may be phagocytic (46, 51). Once phagocytosed, intracellular mycobacteria are likely exposed to the oxidative burst driven by NADPH oxidase homologs found in *Gm* (51), which includes the induction of neutrophil extracellular trap (NET)-like structures known as insect haemocyte extracellular traps (IHET) (52), which were visualised in aggregates of *ex vivo* haemocytes recovered from *MTB* infected *Gm* (**Supplementary Data 3)**. In summary, a comprehensive analysis of the role of the oxidative burst, and the individual role of phagocytic/non-phagocytic haemocytes in MTB defence, requires both markers and methods to differentiate haemocytes and specific innate markers, none of which are currently available.

Histological analysis of *Gm* during H37Rv infection revealed containment of bacilli (both actively replicating and dead/decaying) in GLS of increased frequency, size, and complexity compared to the original model (12). GLS are a generic and non-specific cellular response of *Gm* to isolate non-host material. While the mechanisms are unknown, the formation of GLS is driven by plasmatocytes and granulocytes, sub-types of haemocytes, through a cellular process known as nodulation (37, 38). Encapsulation may follow to contain the primary nodule in a capsule (37). These multi-cellular defence structures have been reported in other *Gm*-bacteria models (e.g., *Mycobacterium abscessus* (33), *Escherichia coli* (53) and *Clostridium perfringens* (54)), and in *Gm*-fungal (e.g., *Candida albican*s (41), *Aspergillus fumigatus* (55)) models. While non-specific, GLS formation is useful to model granuloma-inducing diseases, such as those caused by the MTBC or *Madurella mycetomatis* (56, 57). As the innate immune system of *Gm* can differentiate pathogens and selectively synthesise appropriate AMPs (38), it is likely that GLS have a pathogen-specific composition. This will be testable when suitable reagents (e.g., antibodies and molecular markers) are available. Furthermore, a study into the roles of the remaining four haemocytes: prohaemocytes, spherulocytes, oenocytoids and coagulocytes in innate immune response; and a more comprehensive understanding of how plasmatocytes and granulocytes forms GLS are required for a full characterisation of host biology (58, 59).

Some *Gm*-H37Rv GLS, contained non-ZN-reactive foci. While previously reported in the SAMTB *lux* model (12), H37Rv infection led to more of such foci. The emergence of non-ZN-reactive foci occurred at all stages of infection. Classically, loss of ZN-reactivity is associated with non-replicative bacilli (60), triggered by a switch in phenotype from active to non-replicating (60). Under stress, mycobacteria shorten the lipid chains within the mycolic cell wall (61), and do not retain ZN primary dye (carbol fuchsin) (61). Typically, this is associated with other phenotypic changes, e.g., accumulation of ILIs. However, the intracellular H37Rv in *Gm* lacked ILIs. We hypothesise that H37Rv infection of *Gm* results in both active and non-replicating mycobacterial populations. Future studies to determine the feasibility of *Gm* as an infection model for non-replicating *MTB* will characterise these non-ZN-reactive populations using combinations of auramine-O, polyclonal antimycobacterial antibody, and lipophilic Nile red staining (60, 62, 63).

The *Gm*-H37Rv infection model was evaluated for antimycobacterial drug screening using INH, RIF, ETH and PZA. To address concerns that drug administration 1 h pi may preferentially treat extracellular mycobacteria, the period prior to treatment was extended to 72 h pi, with CFU enumeration at 120 h pi compared to our previous studies with SAMTB *lux* and BCG *lux* (12, 13). CFU enumeration rather than luminescence (which measures metabolic activity) was used as the measure of antimycobacterial activity, because of concern that drug activity can affect metabolic activity and result in inaccurate efficacy data (64).

All treatments, except for PZA, showed significant improvement in larval survival and/or reduction of *in vivo* H37Rv mycobacterial load. Changes in treatment parameters had no effect on the efficacy of INH, RIF, ETH and PZA compared to those reported in the SAMTB *lux* and BCG *lux* drug screening assays (12, 13). RIF and INH were the most efficacious, with activities comparable to use in C3HeB/FeJ and C3H mouse models (65, 66). ETH was efficacious only at 10x the recommended clinical dosage, and our observations align with bacteriostatic activity reported in BALB/C mouse models (67). However, as high concentrations of ETH typically induce bactericidal and not bacteriostatic activity (68), our observations suggest host degradation of ETH or a suboptimal physiological condition for full drug potency. This also aligns with the lack of significant improvement in larval survival outcome following treatment. PZA lacked substantial antimycobacterial activity at all dosages. PZA/POA targets the pantothenate biosynthesis pathway by inhibiting PanD (aspartate decarboxylase)(69). Inhibition of pantothenate biosynthesis disrupts critical metabolic functions (such as fatty acid and ATP synthesis) and is bactericidal (69). However, the abundance of pantothenate (32.8 mg/kg) in *Gm* may allow H37Rv to bypass this PZA inhibition (30). The discrepancy between survival and reduction in mycobacterial burden likely originates from the hypothesised modulation of mycobacterial PDIM by PZA/POA (61). We acknowledge that drug treatment may enhance survival but not necessarily reduce the mycobacterial load in an appropriate manner (as evident with ETH and PZA). Therefore, we recommend that future studies conduct both time-kill and CFU enumeration to minimise risk of generating false positive data.

Comparison of mycobacterial isogenic mutants in animal models is widely used to determine whether a gene of interest encodes a virulence or pathogenicity factor. Here, we show that the *Gm* model can also differentiate *MTB* Δ*phoP* and Δ*dosR* mutants and complemented strains. Deletion of *phoP* from

the PhoPR two-component regulatory system (24, 70) prevents the secretion of ESAT-6 by ESX-1 (71), functionally attenuating virulence. Δ*phoP* was attenuated in *Gm* compared to WT, which was reversible by complementation. The Δ*phoP* attenuation in *Gm* was comparable to that of BCG *lux,* and that found in SCID mice (22).

dosR plays a role in modulating mycobacterial metabolism in the transition from active to non-replicative state, following exposure to intracellular stress (72, 73). Δ*dosR* was more virulent in *Gm* relative to WT in terms of larval death; an effect reversible by complementation. Our results contrast with the majority of Δ*dosR* screening conducted in NHPs, C57BL/6, BALB/C and C3HeB/FeJ mice, guinea pigs and rabbits (25, 26, 28, 29), which reported avirulent or indifferent outcomes. However, our results agree with those in SCID mice, which utilised the same Δ*dosR* strain used in this study (27). Different infection outcomes are likely due to the lack of a *Gm* adaptive immune response. In immune-competent DBA mice, the H37Rv Δ*dosR* mycobacterial load was ~8-10-fold higher than WT during the acute stage of infection (27), but returned to the WT level after induction of the adaptive immune response. Therefore, as both *Gm* and SCID mice lack functional adaptive immune responses, both hosts succumb to infection during the acute stage of infection.

Our results indicate that *Gm* can be used to identify *MTB* virulence genes. However, as highlighted by Δ*dosR*, the results should be interpreted with caution in light of the constraints of the model. Future studies with other mycobacterial mutants known to be attenuated in mammalian models will establish the utility of the method.

This study has highlighted the basic interactions of *Gm* and H37Rv and the data presented should serve as a strong foundation for the adoption and validation amongst the wider TB researching community. While further understanding in the *Gm* immunological responses such as detection of inflammatory markers (e.g., IL-1β and TNF-α), release of necrotic markers (HMGB1) and identification of phagocytic receptors on the haemocytes are needed, we lack the scientific tools required for such studies to take place. This lack of a toolbox is an Achilles heel for *Gm* and one that is widely recognised, and is an area of research that is actively undergoing development to further push the boundaries of this model (74).

In summary, this study highlights the viability of *Gm* as a host for virulent *MTB*, capable of replicating a key aspect of TB infection (e.g. GLS). However, the significance of GLS and its relevance to granulomas observed in other *in vivo* models remains to be determined. We have demonstrated that using different infection parameters *Gm* can differentiate between members of the MTBC in terms of virulence. We have also shown that the *Gm-MTB* model can be used to screen antimycobacterial drugs, and compare isogenic mutants. In both cases the results were comparable to those reported in traditional infection models.

Methods

Mycobacterial strain and growth conditions

Mycobacterial strains utilised in this study are listed in Table 1. Liquid cultures were Middlebrook 7H9 broth (BD, USA), supplemented with 10% albumin dextrose catalase (BD, USA), 0.2% glycerol (Sigma-Aldrich, UK) and 0.05% Tween-80 (Sigma-Aldrich, UK). For solid cultures, mycobacteria were grown on Middlebrook 7H11 agar, supplemented with 10% oleic albumin dextrose catalase (BD, USA) and 0.5% glycerol. Liquid cultures were grown in an orbital shaker at 37 °C at 220 rpm to mid-log phase optical density $(OD)_{600}$ 0.6-0.8 (1 x 10^8 CFU/ml). For growth on agar, plates were incubated in a static incubator at 37 °C with 5% carbon dioxide for 3 weeks.

Acquisition and maintenance of *G. mellonella*

Last (6^{th}) instar *Gm* larvae were purchased from Livefoods Direct (Sheffield, UK). Healthy larvae were selected based on colour (cream lacking melanisation), mass (200-250 mg), size (2-3 cm), and a high level of motility. Dead (non-responsive to physical stimulation) or melanised larvae were discarded. Healthy larvae were stored in vented plastic containers (with wood chippings), in the dark at 18 °C. Larvae were stored for no more than one week and were not fed at any point.

G. mellonella infection with H37Rv, BCG *lux* and SAMTB *lux*

For infection, mid-log phase culture were pelleted at 3000 g for 10 min. Pellets were washed twice in PBS-T (PBS [Sigma-Aldrich, UK] containing 0.05% of Tween-80 [Sigma-Aldrich, UK]). Mycobacteria were adjusted to the desired CFU inocula using OD_{600} measurements of 0.6, 1.5, 8 and 12 as a relative measure for 1 x 10^8, 2 x 10^8, 1 x 10^9, and 2 x 10^9 CFU/ml, respectively. For HT inocula, viable cultures

401 (2 x 10^8 CFU/ml) were incubated in a heated (80 °C) water bath for 1 h. In all experiments, inocula
402 were plated out for CFU to validate the infectious dose.

403

404 Larval infection was carried out as described (11–13, 15, 16). Prior to infection *Gm* were acclimatised
405 to room temperature for 2 h and topically decontaminated using 70% ethanol. *Gm* injection was
406 undertaken on a disposable injection platform of filter paper (for absorption of any leaked
407 haemolymph), taped onto a Petri dish to create a raised platform. Larvae were placed onto the
408 injection platform on their backs and secured using tweezers to expose the pro-legs. Larvae were
409 injected with 10 μl of mycobacterial suspension via the last-left pro-leg using a micro-syringe (25-
410 gauge, SGE Analytical Science, Australia). Infected larvae were transferred from the platform to a Petri
411 dish lined filter paper and incubated in a portable CULTURA mini incubator (Sigma-Aldrich, UK) inside
412 a Class 1 microbiological safety cabinet (MSC), in the dark at 37 °C, for the duration of
413 experimentation.

414

415 **Preparation of antimycobacterial compounds and treatment of H37Rv infected *G. mellonella***

416 Antimycobacterial compounds were purchased from Sigma-Aldrich, UK. For treatment of infected
417 larvae, first-line compounds were prepared according to manufacturer's guidelines for the treatment
418 of adult TB (21), or based on prior *Gm*-MTBC treatment studies (12, 13), relative to the body mass of
419 *Gm* (200 mg): INH (5 mg/kg), RIF (10 mg/kg), ETH (15 or 150 mg/kg) and PZA (25 or 250 mg/kg).
420 Treatment of H37Rv infected (2 x 10^6 CFU) larvae were conducted as described (12, 13) with
421 modifications. Treatment was given as a 10 μl injection via the last right pro-leg, 72 h pi. Treated larvae
422 were incubated for 120 h post-treatment inside a Class 1 MSC in the dark at 37 °C

423

424 ***G. mellonella* survival assay for evaluation of mycobacterial virulence and treatment efficacy**

425 For determination of mycobacterial virulence, larvae were infected, and monitored every 24 h over a
426 192 h time-course (unless otherwise stated), as described (11–13, 15, 16). Infected larvae were
427 considered dead when they failed to respond to physical stimulation. Pupated larvae (the next stage
428 of the *Gm* lifecycle) were discarded and recorded as having survived. Larval survival was similarly
429 recorded for treatment efficacy andpresented as a Kaplan-Meir survival curve, comprised of data
430 generated from three independent experiments unless otherwise stated.

431

Measurement of *in vivo* H37Rv survival in *G. mellonella*

Changes to the bacterial load during infection or following treatment were determined via CFU enumeration. At each time-point, four larvae were randomly selected and individually homogenised in a lysing matrix tube containing six 1/8 inch metal beads in 800 μl of PBS-T, using a FastPrep F120 (MP Biomedicals, USA) at 6.0 m/s for 1 min. For CFU enumeration, serial ten-fold dilutions were plated on Middlebrook 7H11 agar, supplemented with 20 μg/ml of piperacillin (PIP, Sigma-Aldrich, UK) to inhibit the growth of native *Gm* flora (11). PIP has no inhibitory activity on H37Rv (MIC = 320 μg/ml).

Total haemocyte count (THC)

At each time-point, four larvae were bled by piercing the area between the head and the thorax with a 30 gauge needle, and 40 μl from each larva pooled into a 1.5 ml reaction tube containing ice cold insect physiological saline (IPS) (75). IPS maintains near physiological conditions, inhibiting coagulation and/or melanisation. Haemolymph mixtures were pelleted (800 g for 10 min), haemocytes were carefully resuspended in ice cold IPS. Ten micro-litre of cell suspensions were loaded into a disposable counting chamber (VWR, UK), and counted using a light microscope. THCs of naïve and PBS-T mock infected larvae were controls. THCs were derived from three independent experiments.

TEM and histological analysis of *G. mellonella*-*M. tuberculosis* H37Rv interaction

Gm were infected with H37Rv (2 x 10^6 CFU) and processed for TEM and histological analysis as described (11, 12). In brief, for TEM, haemocytes of ten larvae were collected at each time-point and washed as described for THC. Pelleted haemocytes were resuspended in 3% glutaraldehyde, fixed for 10 min, pelleted (800 g for 10 min) and stored at 4 °C. Pelleted haemocytes were treated with 1% osmium tetroxide, dehydrated in ethanol and embedded in resin. Sliced sections (70-90 nm) were mounted, stained with uranyl acetate (0.5%) and lead citrate (3%), and examined using an Tecnai bioTWIN transmission electron microscope (FEI Company, USA). Healthy haemocytes from naïve larvae and suspensions of H37Rv were used as controls. For histological analysis, three larvae were fixed at each time-point by injecting 100 μl of 10% buffered formalin. Fixed larvae were cut into halves along the dorsal line. Larvae were processed for histology using the Sakura Tissue-Tek VIP (Sakura, USA), embedded in paraffin wax using the Histostar™ Embedding Center (Fischer Scientific, USA), and sliced into 4 μm sections using an RM2135 microtome (Leica Biosystems, Germany). Sections were mounted onto glass slides and processed for H&E or ZN staining and examined using an Eclipse 80i light microscope (Nikon, Japan). Uninfected larvae were fixed and used as controls.

Statistical analysis

All data were analysed and plotted using Prism 9 (GraphPad Software Inc, USA). Where appropriate the Mantle-Cox log rank test with Bonferroni's correction, one-way ANOVA with Holm-Šídák multiple comparisons or two-tailed unpaired t-test with multiple comparison correction was used.

Data Availability

The data supporting the findings of this study are available from figshare with DOI:10.6084/m9.figshare.19668768, under open licence (CC BY 4.0). For review please use https://figshare.com/s/3a2e2b5afcf5dc65491d to access the data.

Acknowledgements

This project was funded under the National Centre for the Replacement, Refinement and Reduction of Animals in Research (NC3Rs) PhD studentship (NC/R001596/1) awarded to PRL, SMN, BDR and YL.

References

1. Zhan L, Tang J, Sun M, Qin C. 2017. Animal models for tuberculosis in translational and precision medicine. Frontiers in Microbiology 8:717.
2. Fonseca KL, Rodrigues PNS, Olsson IAS, Saraiva M. 2017. Experimental study of tuberculosis: From animal models to complex cell systems and organoids. PLoS Pathogens 13:e1006421.
3. van Leeuwen LM, van der Sar AM, Bitter W. 2015. Animal models of tuberculosis: Zebrafish. Cold Spring Harbor Perspectives in Medicine 5:a018580.
4. Dionne M, Ghori N, Schneider D. 2003. *Drosphila melonagaster* is a genetically tractable model host for *Mycobacterium marinum*. Infection and Immunity 71:3540–3550.
5. Pagán AJ, Ramakrishnan L. 2018. The formation and function of granulomas. Annual Review of Immunology 36:639–665.
6. Dinh H, Semenec L, Kumar SS, Short FL, Cain AK. 2021. Microbiology's next top model: *Galleria* in the molecular age. Pathogens and Disease 79:ftab006.
7. Gibreel TM, Upton M. 2013. Synthetic epidermicin NI01 can protect *Galleria mellonella* larvae from infection with *Staphylococcus aureus*. Journal of Antimicrobial Chemotherapy 68:2269–2273.

8. Dijokaite A, Humbert MV, Borkowski E, la Ragione RM, Christodoulides M. 2021. Establishing an invertebrate *Galleria mellonella* greater wax moth larval model of *Neisseria gonorrhoeae* infection. Virulence 12:1900–1920.

9. Six A, Krajangwong S, Crumlish M, Zadoks RN, Walker D. 2019. *Galleria mellonella* as an infection model for the multi-host pathogen *Streptococcus agalactiae* reflects hypervirulence of strains associated with human invasive disease. Virulence 10:600–609.

10. Entwistle FM, Coote PJ. 2018. Evaluation of greater wax moth larvae, *Galleria mellonella*, as a novel *in vivo* model for non-tuberculosis mycobacteria infections and antibiotic treatments. Journal of Medical Microbiology 67:585–597.

11. Li Y, Spiropoulos J, Cooley W, Singh Khara J, Gladstone CA, Asai M, Bossé JT, Robertson BD, Newton SM, Langford PR. 2018. *Galleria mellonella* - a novel infection model for the *Mycobacterium tuberculosis* complex. Virulence 9:1126–1137.

12. Asai M, Li Y, Spiropoulos J, Cooley W, Everest D, Robertson BD, Langford PR, Newton SM. 2020. A novel biosafety level 2 compliant tuberculosis infection model using a Δ*leuD*Δ*panCD* double auxotroph of *Mycobacterium tuberculosis* H37Rv and *Galleria mellonella*. Virulence 11:811–824.

13. Asai M, Li Y, Singh Khara J, Robertson BD, Langford PR, Newton SM. 2019. *Galleria mellonella*: an infection model for screening compounds against the *Mycobacterium tuberculosis* complex. Frontiers in Microbiology 10:2630.

14. Mostowy S, Tsolaki AG, Small PM, Behr MA. 2003. The in vitro evolution of BCG vaccines. Vaccine 21:4270–4274.

15. Asai M, Sheehan G, Li Y, Robertson BD, Kavanagh K, Langford PR, Newton SM. 2021. Innate immune responses of *Galleria mellonella* to *Mycobacterium bovis* BCG challenge identified using proteomic and molecular approaches. Frontiers in Cellular and Infection Microbiology 11:619981.

16. Asai M, Li Y, Singh Khara J, Gladstone CA, Robertson BD, Langford PR, Newton SM. 2019. Use of the invertebrate *Galleria mellonella* as an infection model to study the *Mycobacterium tuberculosis* complex. Journal of Visualized Experiments e59703.

17. O'Toole RF, Gautam SS. 2017. Limitations of the *Mycobacterium tuberculosis* reference genome H37Rv in the detection of virulence-related loci. Genomics 109:471–474.

18. Mouton JM, Heunis T, Dippenaar A, Gallant JL, Kleynhans L, Sampson SL. 2019. Comprehensive characterization of the attenuated double auxotroph *Mycobacterium tuberculosis* Δ*leuD*Δ*panCD* as an alternative to H37Rv. Frontiers in Microbiology 10:1922.

19. Kubica G, Kim T, Dunbar F. 1972. Designation of strain H37Rv as the neotype of *Mycobacterium tuberculosis*. International Journal of Systematic and Evolutionary Microbiology 22:99–106.

20. Oatway WH, Steenken W. 1936. The pathogenesis and fate of tubercle produced by dissociated variants of tubercle bacilli. The Journal of Infectious Diseases 59:306–325.

21. World Health Organization. 2010. Guidelines for treatment of tuberculosis, 4th ed. WHO Press, Geneva.

22. Martin C, Williams A, Hernandez-Pando R, Cardona PJ, Gormley E, Bordat Y, Soto CY, Clark SO, Hatch GJ, Aguilar D, Ausina V, Gicquel B. 2006. The live *Mycobacterium tuberculosis phoP* mutant strain is more attenuated than BCG and confers protective immunity against tuberculosis in mice and guinea pigs. Vaccine 24:3408–3419.

23. Pérez E, Samper S, Bordas Y, Guilhot C, Gicquel B, Martín C. 2001. An essential role for *phoP* in *Mycobacterium tuberculosis* virulence. Molecular Microbiology 41:179–187.

24. Gonzalo-Asensio J, Mostowy S, Harders-Westerveen J, Huygen K, Hernández-Pando R, Thole J, Behr M, Gicquel B, Martín C. 2008. PhoP: a missing piece in the intricate puzzle of *Mycobacterium tuberculosis* virulence. PLoS ONE 3:e3496.

25. Converse PJ, Karakousis PC, Klinkenberg LG, Kesavan AK, Ly LH, Allen SS, Grosset JH, Jain SK, Lamichhane G, Manabe YC, McMurray DN, Nuermberger EL, Bishai WR. 2009. Role of the *dosR-dosS* two-component regulatory system in *Mycobacterium tuberculosis* virulence in three animal models. Infection and Immunity 77:1230–1237.

26. Gautam US, Mehra S, Kaushal D. 2015. In-vivo gene signatures of *Mycobacterium tuberculosis* in C3HeB/FeJ mice. PLoS ONE 10:e0135208.

27. Parish T, Smith DA, Kendall S, Casali N, Bancroft GJ, Stoker NG. 2003. Deletion of two-component regulatory systems increases the virulence of *Mycobacterium tuberculosis*. Infection and Immunity 71:1134–1140.

28. Malhotra V, Sharma D, Ramanathan VD, Shakila H, Saini DK, Chakravorty S, Das TK, Li Q, Silver RF, Narayanan PR, Tyagi JS. 2004. Disruption of response regulator gene, *devR*, leads to attenuation in virulence of *Mycobacterium tuberculosis*. FEMS Microbiology Letters 231:237–245.

29. Mehra S, Foreman TW, Didier PJ, Ahsan MH, Hudock TA, Kissee R, Golden NA, Gautam US, Johnson A-M, Alvarez X, Russell-Lodrigue KE, Doyle LA, Roy CJ, Niu T, Blanchard JL, Khader SA, Lackner AA, Sherman DR, Kaushal D. 2015. The DosR regulon modulates adaptive immunity and is essential for *Mycobacterium tuberculosis* persistence. American Journal of Respiratory and Critical Care Medicine 191:1185–1196.

30. Finke MD. 2015. Complete nutrient content of four species of commercially available feeder insects fed enhanced diets during growth. Zoo Biology 34:554–564.

31. Killiny N. 2018. Generous hosts: Why the larvae of greater wax moth, *Galleria mellonella* is a perfect infectious host model? Virulence 9:860–865.

32. Klann AG, Belanger AE, Abanes-de Mello A, Lee JY, Hatfull GF. 1998. Characterization of the *dnaG* locus in *Mycobacterium smegmatis* reveals linkage of DNA replication and cell division. Journal of Bacteriology 180:72.

33. Meir M, Grosfeld T, Barkan D. 2018. Establishment and validation of *Galleria mellonella* as a novel model organism to study *Mycobacterium abscessus* infection, pathogenesis, and treatment. Antimicrobial Agents and Chemotherapy 62:e02539-17.

34. Manca C, Tsenova L, Barry CE, Bergtold A, Freeman S, Haslett PA, Musser JM, Freedman VH, Kaplan G. 1999. *Mycobacterium tuberculosis* CDC1551 induces a more vigorous host response in vivo and in vitro, but is not more virulent than other clinical isolates. Journal of Immunology 162:6740–6746.

35. Yam KC, D'Angelo I, Kalscheuer R, Zhu H, Wang J-X, Snieckus V, Ly LH, Converse PJ, Jr. WRJ, Strynadka N, Eltis LD. 2009. Studies of a ring-cleaving dioxygenase illuminate the role of cholesterol metabolism in the pathogenesis of *Mycobacterium tuberculosis*. PLoS Pathogens 5:e1000344.

36. Wang R, Kreutzfeldt K, Botella H, Vaubourgeix J, Schnappinger D, Ehrt S. 2019. Persistent *Mycobacterium tuberculosis* infection in mice requires PerM for successful cell division. eLife 8:e49570.

37. Dubovskiy IM, Kryukova NA, Glupov VV, Ratcliffe NA. 2016. Encapsulation and nodulation in insects. Invertebrate Survival Journal 13:229–246.

38. Hillyer JF. 2016. Insect immunology and hematopoiesis. Developmental & Comparative Immunology 58:102–118.

39. Nakhleh J, el Moussawi L, Osta MA. 2017. The melanization response in insect immunity. Advances in Insect Physiology 52:83–109.

40. Sigle LT, Hillyer JF. 2016. Mosquito hemocytes preferentially aggregate and phagocytose pathogens in the periostial regions of the heart that experience the most hemolymph flow. Developmental and Comparative Immunology 55:90–101.

41. Sheehan G, Kavanagh K. 2018. Analysis of the early cellular and humoral responses of *Galleria mellonella* larvae to infection by *Candida albicans*. Virulence 9:163–172.

42. Santucci P, Bouzid F, Smichi N, Poncin I, Kremer L, Chastellier C de, Drancourt M, Canaan S. 2016. Experimental models of foamy macrophages and approaches for dissecting the mechanisms of lipid accumulation and consumption during dormancy and reactivation of tuberculosis. Frontiers in Cellular and Infection Microbiology 6:122.

43. Sirakova TD, Dubey VS, Deb C, Daniel J, Korotkova TA, Abomoelak B, Kolattukudy PE. 2006. Identification of a diacylglycerol acyltransferase gene involved in accumulation of triacylglycerol in *Mycobacterium tuberculosis* under stress. Microbiology (N Y) 152:2717–2725.

44. Simeone R, Sayes F, Lawarée E, Brosch R. 2021. Breaching the phagosome, the case of the tuberculosis agent. Cellular Microbiology 23:e13344.

45. Liu J, Tran V, Leung AS, Alexander DC, Zhu B. 2009. BCG vaccines: their mechanisms of attenuation and impact on safety and protective efficacy. Human Vaccines 5:78.

46. Krachler AM, Sirisaengtaksin N, Monteith P, Paine CET, Coates CJ, Lim J. 2021. Defective phagocyte association during infection of *Galleria mellonella* with *Yersinia pseudotuberculosis* is detrimental to both insect host and microbe. Virulence 12:638–653.

47. Tseng YK, Tsai YW, Wu MS, Hou RF. 2008. Inhibition of phagocytic activity and nodulation in *Galleria mellonella* by the entomopathogenic fungus *Nomuraea rileyi*. Entomologia Experimentalis et Applicata 129:243–250.

48. Perini HF, Moralez ATP, Almeida RSC, Panagio LA, Junior AOG, Barcellos FG, Furlaneto-Maia L, Furlaneto MC. 2019. Phenotypic switching in *Candida tropicalis* alters host-pathogen interactions in a *Galleria mellonella* infection model. Scientific Reports 9:1–10.

615 49. Yi Y, Wu G, Lv J, Li M. 2016. Eicosanoids mediate *Galleria mellonella* immune response to
616 hemocoel injection of entomopathogenic nematode cuticles. Parasitology Research 115:597–
617 608.

618 50. Wu G, Yi Y. 2016. Haemocoel injection of PirA1B1 to *Galleria mellonella* larvae leads to
619 disruption of the haemocyte immune functions. Scientific Reports 6:34996.

620 51. Bergin D, Reeves EP, Renwick J, Wientjes FB, Kavanagh K. 2005. Superoxide production in
621 *Galleria mellonella* hemocytes: Identification of proteins homologous to the NADPH oxidase
622 complex of human neutrophils. Infection and Immunity 73:4161–4170.

623 52. Chen RY, Keddie BA. 2021. *Galleria mellonella* (lepidoptera: pyralidae) hemocytes release
624 extracellular traps that confer protection against bacterial infection in the hemocoel. Journal
625 of Insect Science 21:17–18.

626 53. Chen RY, Keddie BA. 2021. The *Galleria mellonella*-enteropathogenic *Escherichia coli* model
627 system: characterization of pathogen virulence and insect immune responses. Journal of
628 Insect Science 21:7–8.

629 54. Kay S, Edwards J, Brown J, Dixon R. 2019. *Galleria mellonella* infection model identifies both
630 high and low lethality of *Clostridium perfringens* toxigenic strains and their response to
631 antimicrobials. Frontiers in Microbiology 10:1281.

632 55. Perdoni F, Falleni M, Tosi D, Cirasola D, Romagnoli S, Braidotti P, Clementi E, Bulfamante G,
633 Borghi E. 2014. A histological procedure to study fungal infection in the wax moth *Galleria*
634 *mellonella*. European Journal of Histochemistry 58:258–262.

635 56. Kloezen W, Poppel M van H, Fahal AH, van de Sande WWJ. 2015. A *Madurella mycetomatis*
636 grain model in *Galleria mellonella* larvae. PLoS Neglected Tropical Diseases 9:e0003926.

637 57. Sheehan G, Konings M, Lim W, Fahal A, Kavanagh K, van de Sande WJ. 2020. Proteomic
638 analysis of the processes leading to *Madurella mycetomatis* grain formation in *Galleria*
639 *mellonella* larvae. PLoS Neglected Tropical Diseases 14:e0008190.

640 58. Pereira TC, Barros PP de, de Oliveira Fugisaki LR, Rossoni RD, Ribeiro F de C, Menezes RT de,
641 Junqueira JC, Scorzoni L. 2018. Recent advances in the use of *Galleria mellonella* model to
642 study immune responses against human pathogens. Journal of Fungi 4:E128.

643 59. Tsai CJ-Y, Loh JMS, Proft T. 2016. *Galleria mellonella* infection models for the study of
644 bacterial diseases and for antimicrobial drug testing. Virulence 7:214–229.

645 60. Vilchèze C, Kremer L. 2017. Acid-fast positive and acid-fast negative *Mycobacterium*
646 *tuberculosis*: The Koch paradox. Microbiology Spectrum 5:TBTB2-0003–2015.

647 61. Bhatt A, Fujiwara N, Bhatt K, Gurcha SS, Kremer L, Chen B, Chan J, Porcelli SA, Kobayashi K,
648 Besra GS, Jacobs WR. 2007. Deletion of *kasB* in *Mycobacterium tuberculosis* causes loss of
649 acid-fastness and subclinical latent tuberculosis in immunocompetent mice. Proc Natl Acad
650 Sci U S A 104:5157–5162.

651 62. Seiler P, Ulrichs T, Bandermann S, Pradl L, Jörg S, Krenn V, Morawietz L, Kaufmann SHE,
652 Aichele P. 2003. Cell-wall alterations as an attribute of *Mycobacterium tuberculosis* in latent
653 infection. The Journal of Infectious Diseases 188:1326–1331.

63. Kapoor N, Pawar S, Sirakova TD, Deb C, Warren WL, Kolattukudy PE. 2013. Human granuloma *in vitro* model, for TB dormancy and resuscitation. PLoS ONE 8:e53657.

64. Baek SH, Li AH, Sassetti CM. 2011. Metabolic regulation of mycobacterial growth and antibiotic sensitivity. PLoS Biology 9:e1001065.

65. Nikonenko B v, Samala R, Einck L, Nacy CA. 2004. Rapid, simple in vivo screen for new drugs active against *Mycobacterium tuberculosis*. Antimicrobial Agents and Chemotherapy 48:4550–4555.

66. Driver E, Ryan G, Hoff D, Irwin S, Basaraba R, Kramnik I, Lenaerts A. 2012. Evaluation of mouse model forming necrotic granulomas using C3HeB/FeJ mice, for the testing of *Mycobacterium tuberculosis* drugs. Antimicrobial Agents and Chemotherapy 56:3181–3195.

67. Zhang T, Li SY, Nuermberger EL. 2012. Autoluminescent *Mycobacterium tuberculosis* for rapid, real-time, non-invasive assessment of drug and vaccine efficacy. PLoS ONE 7:e29774.

68. Zimmerman M, Lestner J, Prideaux B, O'Brien P, Dias-Freedman I, Chen C, Dietzold J, Daudelin I, Kaya F, Blanc L, Chen PY, Park S, Salgame P, Sarathy J, Dartois V. 2017. Ethambutol partitioning in tuberculous pulmonary lesions explains its clinical efficacy. Antimicrobial Agents and Chemotherapy 61:e00924-17.

69. Gopal P, Nartey W, Ragunathan P, Sarathy J, Kaya F, Yee M, Setzer C, Manimekalai MSS, Dartois V, Grüber G, Dick T. 2017. Pyrazinoic acid inhibits mycobacterial coenzyme A biosynthesis by binding to aspartate decarboxylase PanD. ACS Infectious Diseases 3:807–819.

70. Gonzalo-Asensio J, Soto CY, Arbués A, Sancho J, Menéndez MDC, García MJ, Gicquel B, Martín C. 2008. The *Mycobacterium tuberculosis phoPR* operon Is positively autoregulated in the virulent strain H37Rv. Journal of Bacteriology 190:7068–7078.

71. Kumar VA, Goyal R, Bansal R, Singh N, Sevalkar RR, Kumar A, Sarkar D. 2016. EspR-dependent ESAT-6 protein secretion of *Mycobacterium tuberculosis* requires the presence of virulence regulator PhoP. The Journal of Biological Chemistry 291:19030.

72. Zheng H, Williams JT, Aleiwi B, Ellsworth E, Abramovitch RB. 2020. Inhibiting *Mycobacterium tuberculosis* DosRST signaling by targeting response regulator DNA binding and sensor kinase heme. ACS Chemical Biology 15:62.

73. Kendall SL, Movahedzadeh F, Rison SCG, Wernisch L, Parish T, Duncan K, Betts JC, Stoker NG. 2004. The *Mycobacterium tuberculosis dosRS* two-component system is induced by multiple stresses. Tuberculosis 84:247–255.

74. Kling J. 2020. Get a look at *Galleria*. Lab Animal 49:65–67.

75. Maurer E, Hörtnagl C, Lackner M, Grässle D, Naschberger V, Moser P, Segal E, Semis M, Lass-Flörl C, Binder U. 2019. *Galleria mellonella* as a model system to study virulence potential of mucormycetes and evaluation of antifungal treatment. Medical Mycology 57:362.

Figure legends

Figure 1: Virulence and growth of H37Rv in *Gm*. (A) Survival assay of *Gm* (n = 25, per group) challenged with varying infectious doses of H37Rv. Larval survival was recorded every 24 h for 192 h. Mock infected (PBS-T) larvae were included as controls. (B) *In vivo* survival of H37Rv (2 x 10^6 CFU) in *Gm* (n = > 25) was measured over a 192 h time-course. CFU were enumerated from the *Gm* homogenate (n = 4, per time-point) to measure changes in the *in vivo* mycobacterial load over the course of infection. (C and D) survival assay of *Gm* (n = 25, per group) using varying CFU doses of H37Rv, BCG *lux* and SAMTB *lux*, were conducted to determine differences in mycobacterial virulence between the three strains, measured as changes in larval survival. (C) Larval survival was recorded every 24 h for 96 h (1 x 10^7 CFU for BCG *lux* and H37Rv and 2 x 10^7 CFU for SAMTB *lux*) or (D) 192 h (2 x 10^6 CFU). All infected larvae were maintained in the dark at 37 °C following infection. All plotted data are the means of three (or four [Figure 1A, 2 x 10^6 CFU]) independent experiments, and the error bars represent the SD of the means. Sample size per experiment group were n = 25. Percentage represents final larval survival. The Mantle-Cox Log-rank test with Bonferroni's correction, (A) carried out against the mock treated (PBS-T) control or (B) respective H37Rv CFU dose, was used. * = $p < 0.05$, ** = $p < 0.01$, *** = $p < 0.001$ and **** = $p < 0.0001$.

Figure 2: Interaction of H37Rv and *Gm* haemocytes. TEM was undertaken on haemocytes extracted from H37Rv (2 x 10^6 CFU) infected larvae at (A) 1 h, (B) 24 h, (C) 96 h, (D) 144 h and (E) 192 h post-infection (pi). (F) Haemocytes of uninfected larvae and (G) H37Rv were used as the controls. (A) As early as 1 h pi, H37Rv bacilli (blue arrowheads) were internalised by the phagocytic haemocytes. (B) At 24 h pi, small clusters of H37Rv bacilli (blue arrowheads) were contained by aggregates of haemocytes. (C) By 96 h pi, early GLS surrounding a central mass of mycobacteria (highlighted in blue) were visible. (D-E) Abundance of intracellular bacilli (D, highlighted in blue) were observed in increasing frequency with the progression of disease. (E) By 192 h pi, haemocytes were primarily necrotic, losing cell integrity with leakage of intracellular materials and bacilli. N = nucleus. Scale bars represent A, E: 1 µm, C, D: 2 µm, B, F: 4 µm and G: 400 nm.

Figure 3: Formation of granuloma-like structures (GLS) in *Gm* infected with H37Rv. Sagittal histological sections of *Gm* infected with H37Rv (2 x 10^6 CFU) at (A) 24 h, (B) 96 h and (C) 144 h post-infection. ZN stained sections with GLS (black arrows) in increasing abundance and size over the course of infection are shown. FB = fat body, GI = gastrointestinal tract, and red downward triangle = trachea. Scale bar represents 1000 µm.

723

724 **Figure 4: Histological analysis of *Gm*-H37Rv infection.** Histological tissue sections of larvae infected
725 with H37Rv (2 x 10^6 CFU) were prepared and processed for H&E (A, C, E, G, I, and K) or ZN (B, D, F, H,
726 J, and L) staining. Granuloma-like structures (GLS) were visualised at 24 h (A, B), 48 h (C, D), 96 h (E,F)
727 144 h (G, H) 192 h (I-L) post-infection. The complexity of host cell arrangement forming the GLS varied
728 from (A, B) organised to (C, D) unstructured. The physical state of H37Rv bacilli contained within the
729 GLS varied over time with mixtures of individually distinct active clusters of bacilli of varying size
730 (bright pink) or densely packed highly ZN-reactive amorphous material released from dead/dying
731 bacilli (dark purple). Loss in ZN affinity (grey mass) was observed in structures 96 h pi onwards (F, J, L).
732 Cell necrosis, visible in H&E stained sections characterised by cellular fragmentation, loss/fading of
733 nuclear staining, and decreased staining (due to appearance of pale spongy pockets) were observed
734 in the areas associated with densely packed ZN reactive material. Scale bars represents 20 µm for A,
735 B, E, and F; 100 µm for C, D and G-I; 50 µm for K and L.
736

737 **Figure 5: Unique varieties of granuloma-like structures (GLS) found in *Gm* infected with H37Rv.**
738 Magnified images of ZN and H&E stains presented in Figure 4, highlighting key areas of interest. (A)
739 large aggregates of individually distinct H37Rv bacilli were observed (ZN, circumscribed by black
740 dotted line). A GLS clearly defined as circular eosinophilic area with faded spongy pockets of staining
741 (H&E, circumscribed by white dotted line). (B) A GLS containing dense ZN reactive material, with
742 localised peripheral loss in ZN reactivity as indicated in the area enclosed by the black square. Foci of
743 intense H&E staining most likely indicates host cell necrosis. (C) A GLS associated with predominant
744 loss of ZN reactivity. In contrast to (B), non-ZN reactive masses were associated with less intense H&E
745 staining, and host cell nuclei were more easily distinguishable (as highlighted by the white arrows);
746 likely indicating that the level of host cell necrosis is low despite the presence of mycobacterial mass.

747

748 **Figure 6: Changes in the total number of circulating haemocytes in *Gm* infected with H37Rv.** (A) The
749 total haemocyte count (THC) was measured from H37Rv (2 x 10^6 CFU), PBS-T (mock infected), or naïve
750 larvae (n = 4, per time-point) every 24 h over a 192 h time-course, with the exception of 120 h post-
751 infection (pi). Plotted are the means of three independent experiments, and the error bars represent
752 the SD of the means. (B) Changes in THC, relative to larval mortality (as presented in Figure 1A) and *in*
753 *vivo* H37Rv load (as presented in Figure 1B) of infected larvae (2 x 10^6 CFU) over the course of 192 h
754 time-course. Suppression of THCs within the first 96- h pi, indicates diversion of circulating

haemocytes into sessile state as GLS are formed. However, containment does not eliminate infection, as indicated by the proliferation of H37Rv bacilli during the corresponding time-points. By 96-192 h pi, GLS succumb to the replicating bacilli, leading to a breach in containment, inducing further immune responses as indicated by the rise in THCs back to the t = 0 h level. Nevertheless, the immune response is overloaded by the growth of H37Rv, inducing larval mortality, as indicated by the increase rate of larval mortality over the corresponding time-points.

Figure 7: Treatment of H37Rv infected *Gm* using clinically recommended antimycobacterial compounds. Larvae (n = 25) were infected with H37Rv (2 x 10^7 CFU) and treated using one of the following antimycobacterial compounds: INH (5 mg/kg), RIF (10 mg/kg), ETH (150 mg/kg) or PZA (250 mg/kg) using concentrations recommended for treatment of adult TB, scaled relative to body mass of the larva (200 mg). ETH and PZA were used at 10x the recommended dosage. Infection was allowed to establish for 72 h prior to treatment. Following infection, larvae were incubated in the dark at 37 °C. (A) INH or RIF treated larvae showed significant improvements in larval survival relative to the mock treated (PBS-T) controls. Larval survival was monitored every 24 h for 120 h post-treatment (or 192 h inclusive of incubation period). (B) All treatments (with the exception of PZA) led to a significant reduction in *in vivo* H37Rv burden (%), measured via CFU enumeration of H37Rv from homogenised *G. mellonella* (n = 4, per time-point). Plotted are the means of (A) three or (B) five independent experiments, and the error bars represent the SD of the means. (A) The Mantle-Cox log-rank test with Bonferroni's correction was carried out against the mock treated (PBS-T) controls. (B) One-way ANOVA test with Holm-Šídák multiple comparisons between PBS and treatment: **** (black) = $p < 0.0001$, degree of freedom = 4 and F-value = 43.79. Two tailed unpaired student's t-test between PT and treatment: *** (red) = $p < 0.001$ **** (red) = $p < 0.0001$.

Figure 8: Determining virulence of isogenic mutants Δ*phoP* and Δ*dosR* against H37Rv wild-type in *Gm*. Larvae (n = 25, per group) were challenged with (A) Δ*phoP* or Δ*phoP* complement (Δ*phoP* comp), (B) Δ*dosR* or Δ*dosR* complement (Δ*dosR* comp). Larvae infected with H37Rv wild-type (WT) were utilised as the virulence control. Virulence was assessed via larval survival assay over a 192 h time-course. Infected larvae were maintained at 37 °C in the dark, and survival was recorded every 24 h. All data plotted are the mean of three independent experiments. Percentage represents final larval survival. Error bars represents the SD of the means. The Mantle-Cox log-rank test with Bonferroni's correction was conducted against the WT. ** = $p < 0.01$ and **** = $p < 0.0001$.

Mycobacteria	Additional supplement for selection	Source
MTB H37Rv TMC 102/ATCC 35837 (H37Rv)	None	ATCC, USA
MTB H37Rv Δ*leuD* Δ*panCD* pMV306hsp+*Lux* (SAMTB *lux*)	Hygromycin* (50 μg/ml) Kanamycin^ (20 μg/ml) Leucine^ (25 mg/ml) Pantothenate^ (24 μg/ml)	Prof. William Jacobs Jr. (Albert Einstein College of Medicine, USA)
M. bovis BCG Montréal vaccine pSMT1 (BCG *lux*)	Hygromycin* (50 μg/ml)	Prof. Douglas Young (Imperial College London, UK)
MTB H37Rv Δ*phoP*	Hygromycin* (50 μg/ml)	(70)
MTB H37Rv Δ*phoP* complement	Hygromycin* (50 μg/ml) Kanamycin^ (20 μg/ml)	(70)
MTB H37Rv Δ*dosR*	None	(27)
MTB H37Rv Δ*dosR* complement	None	(27)

Table 1: List of mycobacterial strains utilised in this study

List of mycobacterial strains utilised, the additional supplements required for growth (* Roche Diagnostics, USA; ^ Sigma-Aldrich, UK) and the source of strains.

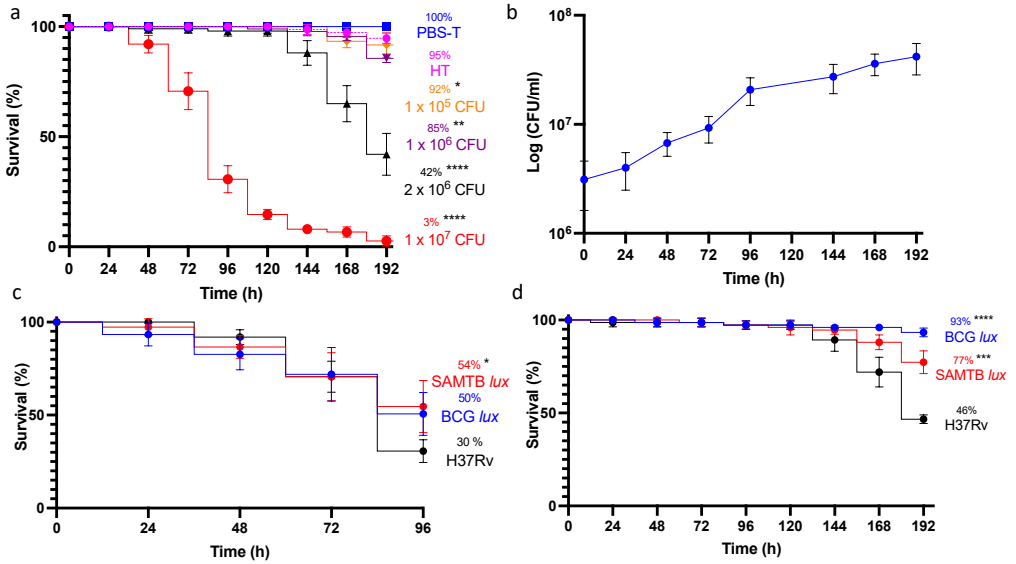

792

793 **Figure 1**

794

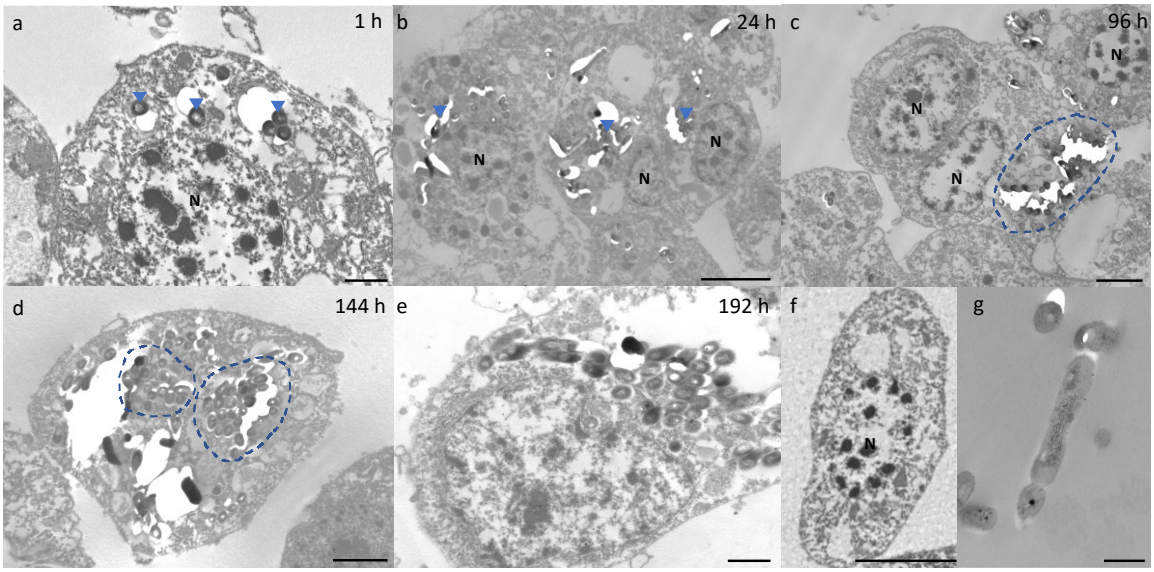

795

796 **Figure 2**

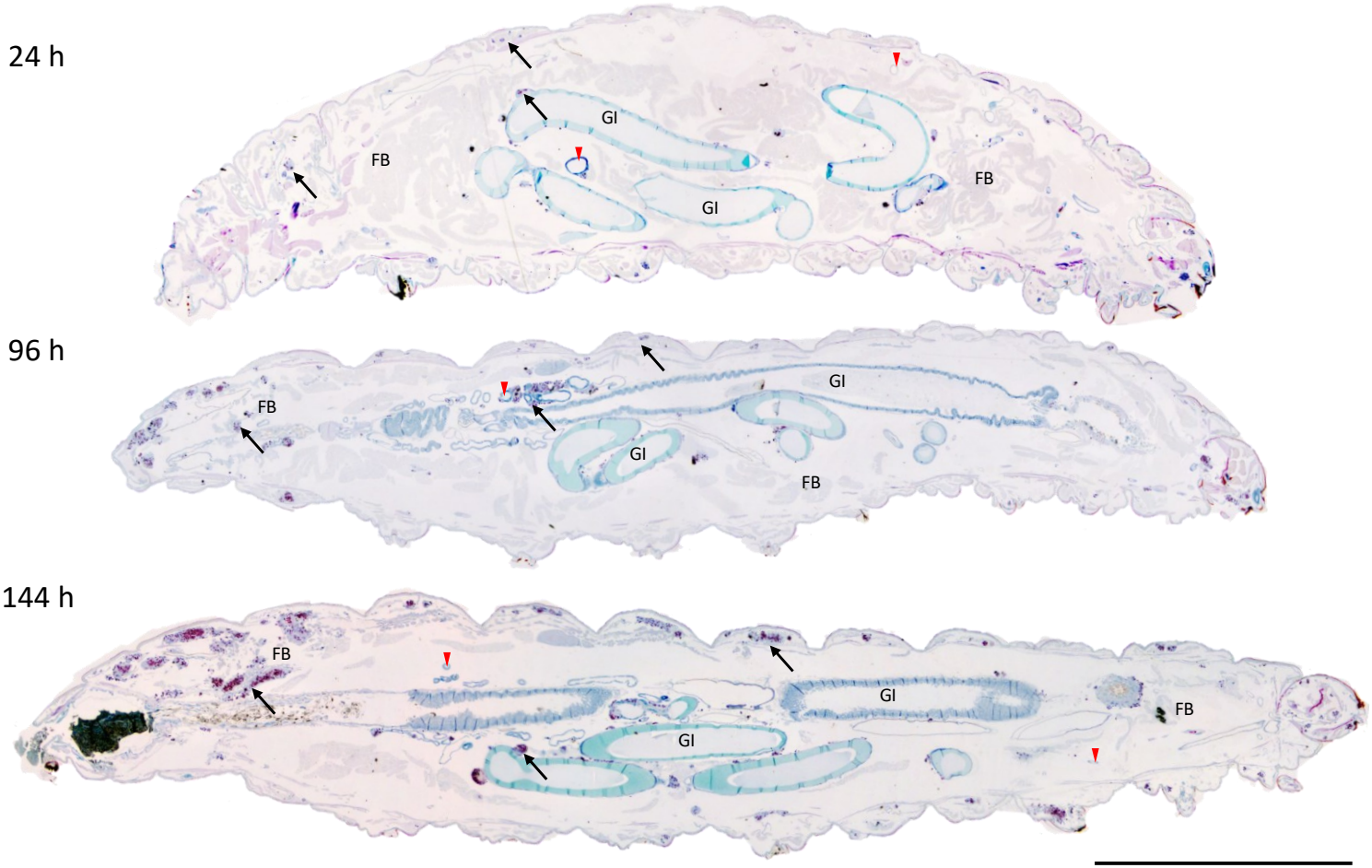

797

798 **Figure 3**

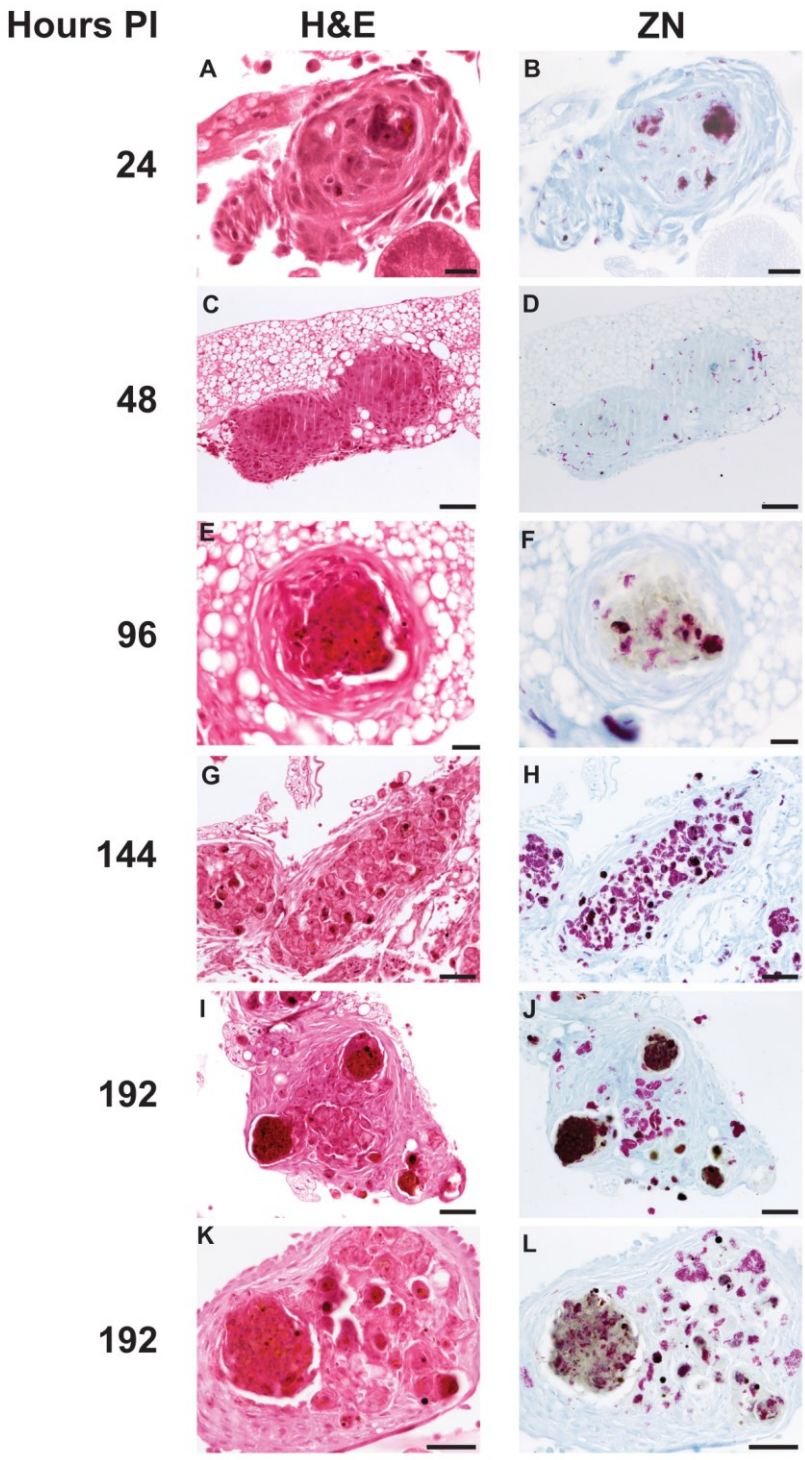

799

800 **Figure 4**

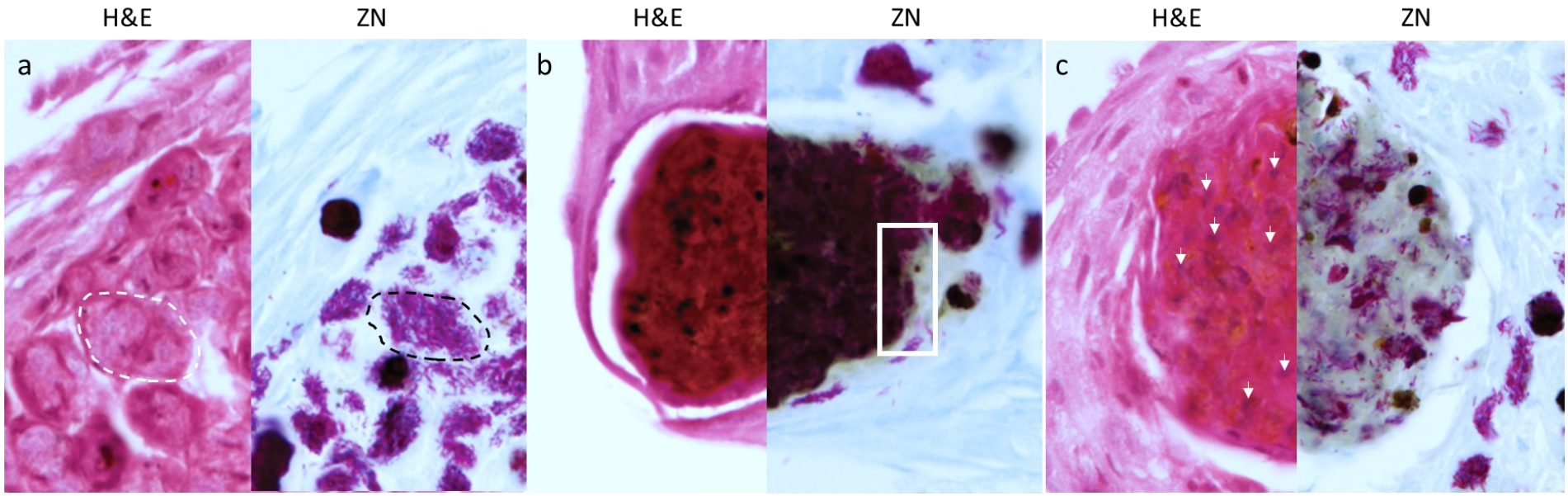

Figure 5

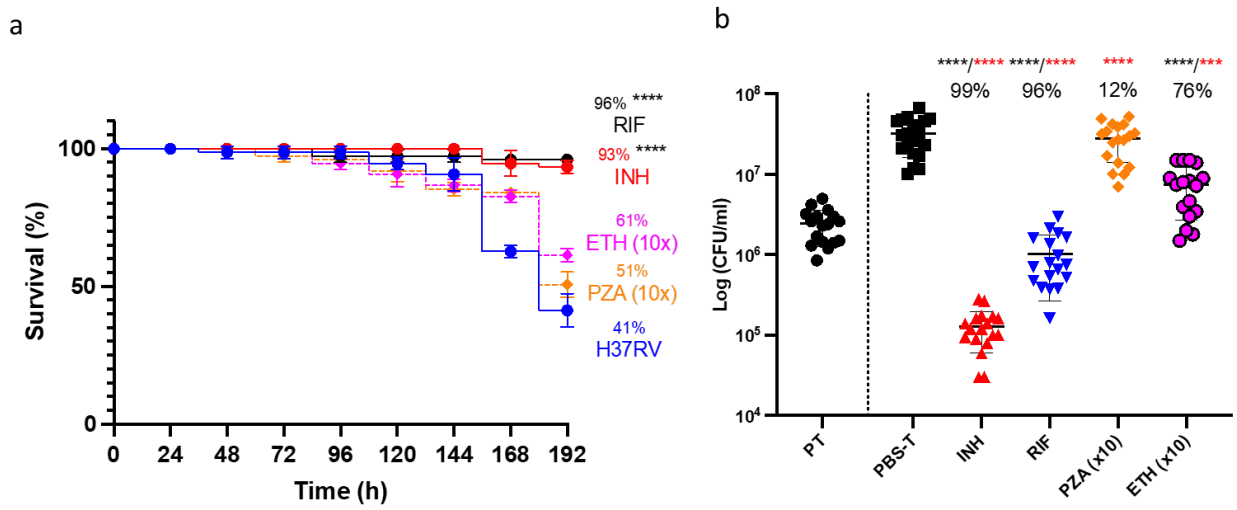

803

804 **Figure 6**

805

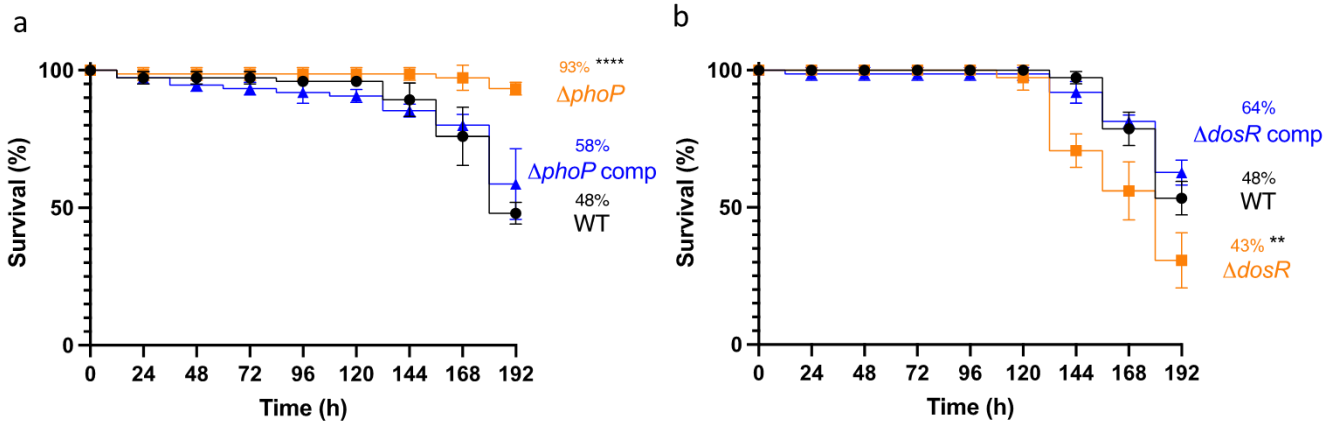

806

807 **Figure 7**